

Thermal radiation anomalies associated with major earthquakes

Dimitar Ouzounov¹, Sergey Pulinetz², Menas C. Kafatos¹ and Patrick Taylor³

¹Chapman University, CEESMO, Orange, CA, USA.

²Space Research Institute, RAS, Moscow, Russia.

³NASA GSFC, Greenbelt, MD, USA.

Corresponding author: Dimitar Ouzounov (Ouzounov@chapman.edu)

Key Points:

- Identify a method of recognition for pre-earthquake thermal radiation anomalies.
- Estimate of thermal energies associated with some large earthquakes.
- Described a mechanism for pre-earthquake thermal radiation anomalies generation.

29
30
31
32
33
34
35
36
37
38
39
40
41
42
43
44
45
46
47
48
49
50
51
52
53
54
55
56
57
58
59
60
61
62
63
64
65
66
67
68
69
70
71
72
73
74
75
76
77
78
79
80
81

Abstract

Recent developments of remote sensing methods for Earth satellite data analysis contribute to our understanding of earthquake related thermal anomalies. It was realized that the thermal heat fluxes over areas of earthquake preparation is a result of air ionization by radon (and other gases) and consequent water vapor condensation on newly formed ions. Latent heat (LH) is released as a result of this process and leads to the formation of local thermal radiation anomalies (TRA) known as OLR (outgoing Longwave radiation, Ouzounov et al, 2007). We compare the LH energy, obtained by integrating surface latent heat flux (SLHF) over the area and time with released energies associated with these events. Extended studies of the TRA using the data from the most recent major earthquakes allowed establishing the main morphological features. It was also established that the TRA are the part of more complex chain of the short-term pre-earthquake generation, which is explained within the framework of a lithosphere-atmosphere coupling processes.

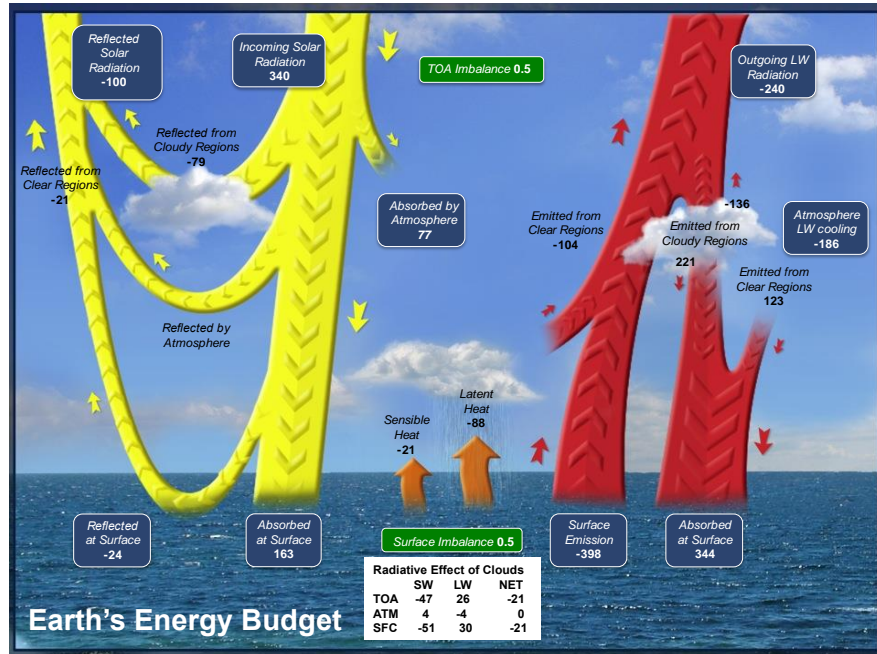
List of Acronyms:

AVHRR- Advanced Very High Resolution Radiometer(NOAA)
ACP- Atmospheric chemical potential
EMSC- European-Mediterranean Seismological Centre
EOS - Earth Observation System (NASA)
AIRS –Atmospheric Infrared Sounder (NASA)
EQ-earthquake
GMSD –IGS GPS station in Japan
GOES - Geostationary Operational Environmental Satellite (NOAA)
ISTF- Integrated satellite and terrestrial framework
LAIC- Lithosphere-Atmosphere-Ionosphere Coupling
LH – Latent heat
LWR – Long wave radiation
LAIMC - Lithosphere-Atmosphere-Ionosphere-Magnetosphere Coupling
POES - Polar Operational Environmental Satellites (NOAA)
OLR –Outgoing Longwave Radiation
RST- Robust Satellite technique
STIR- Satellite thermal infrared radiation
SW –short wave radiation
TIR-Thermal Infrared radiation
TOA – Top of the Atmosphere
USGS-US Geological Survey

1. Introduction

The search for physically based pre-seismic signals has been conducted for many years (e.g., Martinelli, 1998). Multiple observations of earthquake precursory signals have previously been published (Hayakawa M, (Ed), 1999, Hayakawa M. and O.A.Molchanov (Ed), 2002, Pulinets and Boyarchuk, 2004). Recent analyses of data from multi-instrument space-borne and ground observations have provided evidence for the existence of pre-earthquake atmospheric signals (Han et al, 2014, 2016, Hayakawa (Ed) 2012, Kon et al, 2010 , Liu et al 2000, 2010, Tramutoli et al, 2015a,b,, Ouzounov et al, 2011 , Pulinets and Davidenko, 2014) These studies have contributed to our understanding of the physics of earthquakes and the phenomena that precede their energy release. Recent advances in earth observing space technology have also helped to advance the scientific understanding of the nature of pre-earthquake phenomena in the atmosphere. We are searching for pre-seismic observations that might give warning of a major earthquake. Our investigation is

82 based on a search for possible connection between satellite observations (latest NPOESS -
 83 National Polar-orbiting Operational Environmental Satellite System and NASA EOS -
 84 Earth Observing System) of anomalous atmospheric thermal transient signals and
 85 subsequent major earthquakes.



104
 105 *Fig. 1. Earth Atmospheric Energies, (Earthobservatory.nasa.gov, NASA, 2012)*

106 Figure 1, the Earth's Energy Budget (Earthobservatory.nasa.gov), shows that more than
 107 70% of the reflected solar radiation occurs in the atmosphere. While the Earth surface
 108 absorbs incident shortwave (SW) solar energy nearly one third is reflected back into
 109 space. The heat absorbed at the surface does not reach any significant depth because the
 110 surfaces low thermal conductivity. The absorbed energy instead is re-emitted as long
 111 wavelength radiation (LWR) energy mostly during the nighttime.

112 The energy directly released into the atmosphere, is known as sensible heat (SH)- and is
 113 transferred as radiant thermal energy or heat. This latent heat (LH) is the energy released
 114 or absorbed by a substance during a phase change. A balance must exist between
 115 incoming and radiated solar energy or else the surface of Earth would permanently heat
 116 up. This process of radiative exchange is complex. Generally the LWR emitted by the
 117 Earth into the atmosphere gets absorbed and maintains a thermal equilibrium with the
 118 atmosphere. When the sky is clear the LWR escapes into space since the atmosphere is
 119 "transparent" to the radiation in the 8.0-12.0 μm spectral wavelengths. Sometimes this
 120 atmospheric window can be partially blocked by clouds or pollution and outgoing LWR
 121 could be reabsorbed by the atmosphere and re-emitted in all directions.

122 The outgoing LWR at the top of the atmosphere (TOA) has been estimated by satellite
 123 sensors as outgoing long wave radiation (OLR). The net result is that radiative losses
 124 from the atmosphere are generally balanced by the energy re-emitted as heat from Earth's
 125 surface. Later, mainly during the formation of clouds, the water vapor condensates and the
 126 LH is released into the atmosphere (estimated by SLHF from NCEP). This leads to heat
 127 transfer from the surface into the atmosphere, which is one of the main drivers of the
 128 general, atmospheric circulation (Goosse et al, 2016)

129
 130 **2.Methods for recognition of thermal radiation anomalies (TRA)**

131 For more than 2000 years scientists have been searching for signals preceding
 132 earthquakes. According to ancient Greek philosopher Aristotle, "pneuma" (wind/gas) are
 133 involves before earthquakes producing strange atmospheric effects (MacArthur, 1980).
 134 The fundamental meaning of "pneuma" is air in motion or electricity in the airs. Fogs and

135 clouds were recognized as observational evidence for activities prior to major seismicity
136 since the days of Aristotle and Pliny (Roman Empire) and many researchers in ancient
137 China (Tributsch, 1978). John Milne - an English seismologist and geologist who invented
138 the first modern seismograph has published the first quantitative analysis of atmospheric
139 signals associated with seismicity (Milne, 1913). He found that for 387 earthquakes in
140 Northern Japan, the sinuses of the curves of means monthly temperature were generally a
141 little ahead of the crest of the waves indicating the earthquake arrival (Milne, 1913).

142 Just recently a comprehensive catalog of atmospheric pre earthquake signals based on
143 historical and instrumental record for more than 1500 earthquakes between 550 BA until
144 2000AD been published (Tronin, 2011). Several atmospheric parameters (atmospheric
145 heat, drought, cooling, clouds, air pressure variations, winds, fogs, etc.) have been found
146 before the seismic shocks occurrence related to about 700 earthquakes (~50% from the
147 all cases) and only temperature increased been seen in 10% of the cases , which is still a
148 good indicator, having in mind the thermometer been invented only in 16th century. In
149 addition to the atmospheric phenomena variety of hydrological changes been reported
150 usually followed by gas release (bad smell) and foggy atmosphere (Tronin, 2011).

151
152 The recent advances in remote sensing instruments have helped to advance the scientific
153 understanding of atmospheric earthquake signals. Satellite thermal imaging data reveal
154 stationary (long-lived) thermal anomalies associated with large linear structures and fault
155 systems in the Earth's crust (Carreno et al., 2001) but also transient (short-lived)
156 anomalies prior to major earthquakes (Qing et al., 1991, Salman et al., 1992). Their
157 spatial extent and temporal evolution may be dependent on local geology and tectonics,
158 nature of the focal mechanism, meteorological conditions and other factors. Studies on the
159 relationship between satellite thermal infrared (TIR) data and earthquake precursors have
160 been based on data from both single and multi-instruments . Gorny et al. (1988), Tronin et
161 al. (2002,2004), Dey et al. (2004), Saraf et al, (2005) have used imagery recorded by
162 Advanced very-high-resolution radiometer (AVHRR), analysis methods based on a
163 comparisons between before and after images over an an earthquake epicenter. Newer
164 techniques have been proposed, using sub-pixel level co-registration and geo-referenced
165 data from both polar-orbiting and geosynchronous satellites (GOES, Meteosat, AVHRR,
166 and Landsat (Bryant et al., 2003; Di Bello et al., 2004).One of the problems in detecting
167 TIR anomalies is defining abnormal TIR fluctuations from a normal baseline. To address
168 this problem, an approach was developed using a time series of TIR data over earthquake
169 prone regions. Using pixel-level thermal radiation variance from established base lines, it
170 was possible to identify anomalous TIR signals (Tramutoli et al., 2001, Filizzola et al.,
171 2004, Cervone et al., 2006, Ouzounov et al, 2007). After the launch of the EOS satellites
172 (1999-Terra and 2002-Aqua), a new approach for detecting pre-earthquake anomalies was
173 developed, based on Land Surface Temperature (LST) derived from the 11-micron data
174 (Ouzounov and Freund, 2004). Observations with NPOESS and the EOS Aqua's
175 Atmospheric Infrared Sounder (AIRS) of atmospheric environmental parameters have
176 revealed an increase in radiation and a transitional change in Outgoing Longwave
177 Radiation (OLR) in the 8-12 micron range (Ouzounov et al., 2007). OLR transitional
178 changes recorded at the TOA (top of the atmosphere) over seismically active regions have
179 been proposed as being related to thermodynamic processes within the earth's crust that
180 lead to earthquakes (Ouzounov et al., 2011; Pulinets and Ouzounov, 2011).

181 182 **2.1 Robust Satellite technique**

183 Space-time anomalies of Earth's emitted radiation in the thermal infrared spectral range
184 (TIR) measured from satellite months to weeks before an earthquakes, have been
185 interpreted, by several authors, as pre-earthquake signals (Qiang et al., 1991; Tronin ,
186 1996,2006; Gorny et al. 1988;Tramutoli et al., 2005).

135
136
137
138
139
140
141
142
143
144
145
146
147
148
149
150
151
152
153
154
155
156
157
158
159
160
161
162
163
164
165
166
167
168
169
170
171
172
173
174
175
176
177
178
179
180
181
182
183
184
185
186
187

188
189
190
191
192
193
194
195
196
197
198
199
200
201
202
203
204
205
206
207
208
209
210
211
212
213
214
215
216
217
218
219
220
221
222
223
224
225
226
227
228
229
230
231
232
233
234
235
236
237
238
239
240
241

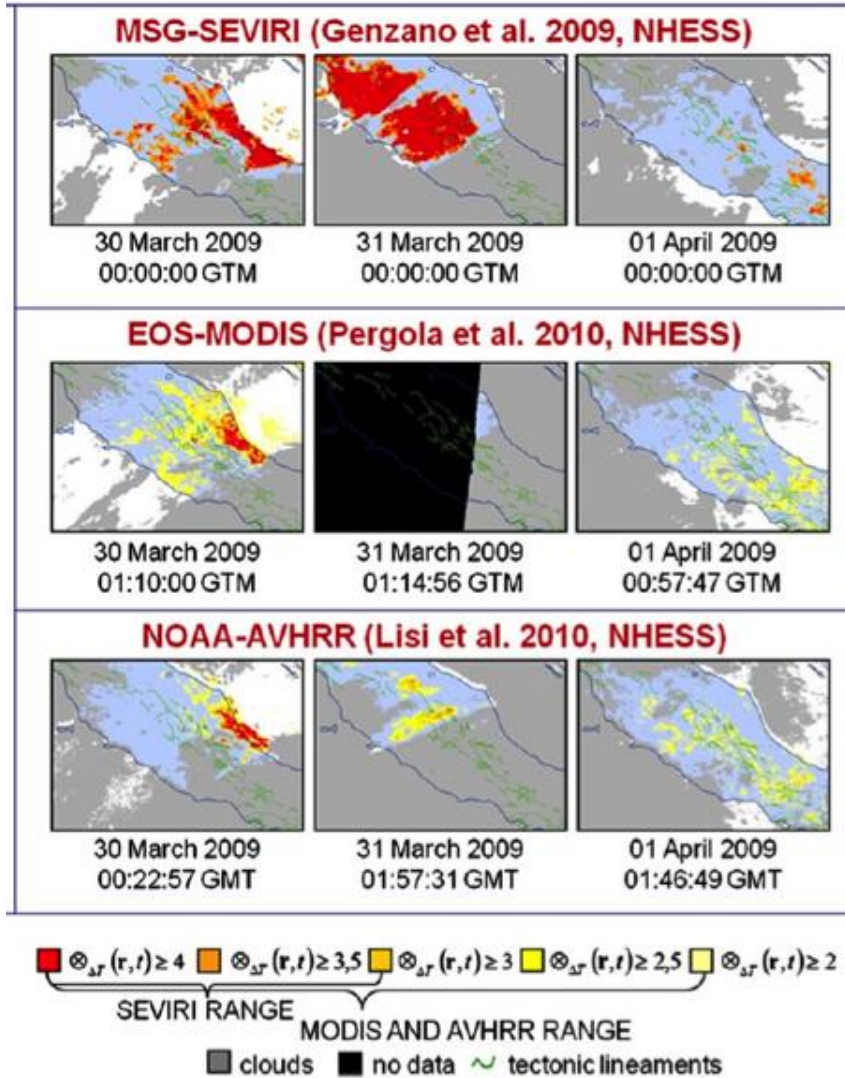


Fig.2 RST application for seismically active areas show space-time correlation between thermal anomalies and earthquakes occurrence. The case of L'Aquila earthquake (6 April 2009, M_w 6.3) by using (top to bottom) both polar (Lisi et al., 2010; Pergola et al., 2010 for NOAA/AVHRR and EOS/MODIS) and geostationary (MSG/SEVIRI, Genzano et al., 2009) sensors respectively.

The claimed connection of TIR emission with seismic activity has been considered, for a long time with some caution, by the scientific community mainly because of the insufficiency of validated data-sets and the scarce importance attached by those authors to other causes (e.g. meteorological) that, rather than seismic activity, could be responsible for the observed TIR signal fluctuations (for a review see Tramutoli et al., 2015a,b and reference herein). The Robust Satellite technique (RST) technique is based on a preliminary multi-temporal analysis on several years of homogeneous historical dataset of satellite TIR records, which are devoted to interpreting the TIR signal for each pixel of the satellite observations. Anomalous TIR patterns are identified using a specific index, RETIRA (Robust Estimator of TIR Anomalies, Filizzola et al., 2004; Tramutoli, 2005). Quality of TIR data analyses and of the validation processes devoted to assess the possible correlation among TIR anomalies and seismic activity have been improved in recent years (Tramutoli et al., 2015b), increasing the possibility of including them among the observables which are expected to positively contribute to an advanced multi-parametric system for a time-Dependent Assessment of Seismic Hazard (Elefteriou et al., 2015, Tramutoli et al., 2014a, 2014b). In particular, the Robust Satellite data analysis Technique (RST) proposed in 1998 by Tramutoli (see also Genzano et al, 2007) has been successfully

applied in order to identify pre-earthquake space–time TIR anomalies even in very variable observational (satellite view angle, land topography and coverage, etc.) and normal (e.g. meteorological) conditions. In subsequent RST applications to different seismically active areas, the space-time correlation between thermal anomalies and earthquakes occurrence was confirmed. For instance by using both polar (Lisi *et al.*, 2010; Pergola *et al.*, 2010 for NOAA/AVHRR and EOS/MODIS respectively) and geostationary (MSG/SEVIRI, Genzano *et al.*, 2009) sensors, in the case of L'Aquila earthquake (6 April 2009, M_w 6.3). (See Fig.2)

2.2 Outgoing long wave radiation analysis

One of the main parameters used to characterize the Earth's radiation environment is outgoing long-wave-earth radiation (Liebmann and Smith, 1996). OLR has been associated with the top of the atmosphere integrating the emissions from the ground, lower atmosphere and clouds (Ohring G. and Gruber, 1982) and primarily was used to study Earth radiative budget and climate studies (Gruber and Krueger, 1984). Daily OLR data were used to study the OLR variability in the zone of earthquake activity (Liu and Kang 1999; Ouzounov *et al.*, 2007, 2011; Xiong *et al.*, 2010). An increase in radiation and a transient change in OLR was proposed to be related to thermodynamic processes in the atmosphere over seismically active regions and described as thermal radiation anomaly (TRA). Because of today varieties in OLR type of algorithms and data products such as: RBUD – NOAA/CLASS; CERES LWR – TOA fluxes; NOAA/AVHRR –OLR, and EOS Aqua -CLROLR fluxes; we introduce the thermal radiation anomaly (TRA) as a common name for type of anomalies based on different data for computing the transitional LWR. The anomalous characteristic of TRA was suggested by Ouzounov *et al.*, (2007) as a statistical maximum change in the rate of OLR for a specific spatial location and predefined times and was constructed corresponding to the anomalous thermal field (Tramutoli *et al.*, 1999, 2013). The anomaly represents the different amplitude for a specific spatial location and predefined times:

$$\text{Anomaly } (x, y, t) = \frac{S(x,y,t) - \bar{S}(x,y,t)}{\tau(x,y,t)} \quad (1)$$

$$\bar{S}(x, y, t) = \frac{1}{N} \sum_{i=1}^N S(x_i, y_i, t_i) \quad (2)$$

$$\tau(x,y,z) = \sqrt{\frac{\sum (S(x,y,t) - \bar{S}(x,y,t))^2}{N}} \quad (3)$$

Where: $S(x, y, t)$ the current OLR value, $\bar{S}(x, y, t)$ the computed mean of the background field, defined as the daily y mean value of OLR $S(x_i, y_i, t_j)$ over an area of longitude x and latitude y in the t^{th} day of the M years and $\tau(x,y,z)$ the standard deviation over the same location (x,y) and local time (t) as OLR value. This rapid enhancement of radiation could be explained by an anomalous flux of the latent heat over the area of increased tectonic activity. The input data been processed in the native resolution of (2.5x2.5) and the output maps been processed in two steps procedure.: 1/ Grid resolution enhancement (1x1 degree) with additional pre-processing for avoiding aliasing of short wavelengths; and 2/ Re gridding with spatial filtering and grid points re computing based on “minimum curvature” algorithm used by standard computation packages (Fisher *et al.*, 2008).

In our studies, we used OLR data from NCEP/NOAA's Advance Radiation Radiometer (AVHRR). A daily mean global data base, with a spatial resolution of 2.5° by 2.5°, was used to study the OLR activity and variability in the region of three recent major earthquakes: i/ M7.1 on October 24, 2011 in Van, Turkey; ii/ M6.9 on May 24, 2014 Aegean Sea, Greece and iii/ M6.0 on August 24, 2014 in Napa, CA (See Table 1)

293
294

Table 1. List of studied earthquakes (USGS)

	Name	Date (mm/dd/yyyy)	Geographic lat/lon (°)	Time (UTC)	M	H (km)
1	Van, Turkey	10/25/2011	38.62 N/43.48 E	16:41:00	7.2	7.1
2	Aegean Sea, Greece	05/24/2014	40.3 N/25.45 E	09:25:00	6.9	10
3	NapaValley, California,US	08/24/2014	38.21 N/122.31W	10:24:44	6.0	11.11

295

296

297

298

299

300

301

302

303

304

305

306

307

308

309

310

311

312

313

314

315

316

317

318

319

320

321

322

323

324

Our method includes recording the OLR at the top of the atmosphere several days before the onset of an earthquake and characterizes the state of the atmosphere before the earthquake by the established baseline. Calculated at the TOA, OLR from NOAA POES were used to study the Earth's radiation budget, because they represent emissions from the Earth's surface, lower atmosphere, and clouds, and they are sensitive to near surface and cloud temperatures. Observations from the NOAA POES were based on the long-wave flux estimation of Ellingson et al. (1989). Daily mean OLR values were calculated from these raw data, using algorithms based on Eqs. (1-3) and customized for each region. The NOAA Climate Prediction Center (<http://www.cdc.noaa.gov/>) provides daily and monthly OLR data and the OLR algorithm for analyzing the advanced very high-resolution radiometer (AVHRR) data. A daily mean, covering a significant area of the Earth (90° N–90° S, 0° to 357.5° E) and with a spatial resolution of 2.5° x 2.5° recorded.

The “daily values”, “normal state” and “TRA anomalies” in relation to pre-earthquake OLR signals were introduced initially by Ouzounov et al., 2007 and Xiong et al. 2010. The “TRA anomaly” has been calculated as a deviation of daily values from the normal state and normalized by the multiyear standard deviation for the same pixel (Eq.1) and shown on Fig.3, 4, and 5 in red. The “Daily values” are daily raw values of OLR for the same pixel and same local time observed by the polar orbit satellite Figs. 3,4, and 5 (gray curve line). The “normal state” for OLR was estimated by a multiyear average (from 2004 to the present) for each pixel (Eq.2) and Figs.3,4, and 5 (black solid curve). The OLR “anomalies” represent the maximum change in the daily variations of the OLR in comparison to the “normal state”.

The continuous satellite monitoring of OLR data over Turkey, shows a rapid increase of emitted radiation during mid the September- October 2011 time frame (Fig. 3). An anomaly at TOA was detected at 19:00 LT on October 19, 2011, south east of the epicenter area. The anomaly was spatially extended and temporally persistent for 8 hours and was the largest TRA anomaly over the entire European continent at that time (Ouzounov et al., 2014).

325

326

327

328

329

330

331

332

333

334

335

336

337

338

339

340

341

342

343

344

345

346

347

348

349

350

351

352

353

354

355

356

357

358

359

360

361

362

363

364

365

366

367

368

369

370

371

372

373

374

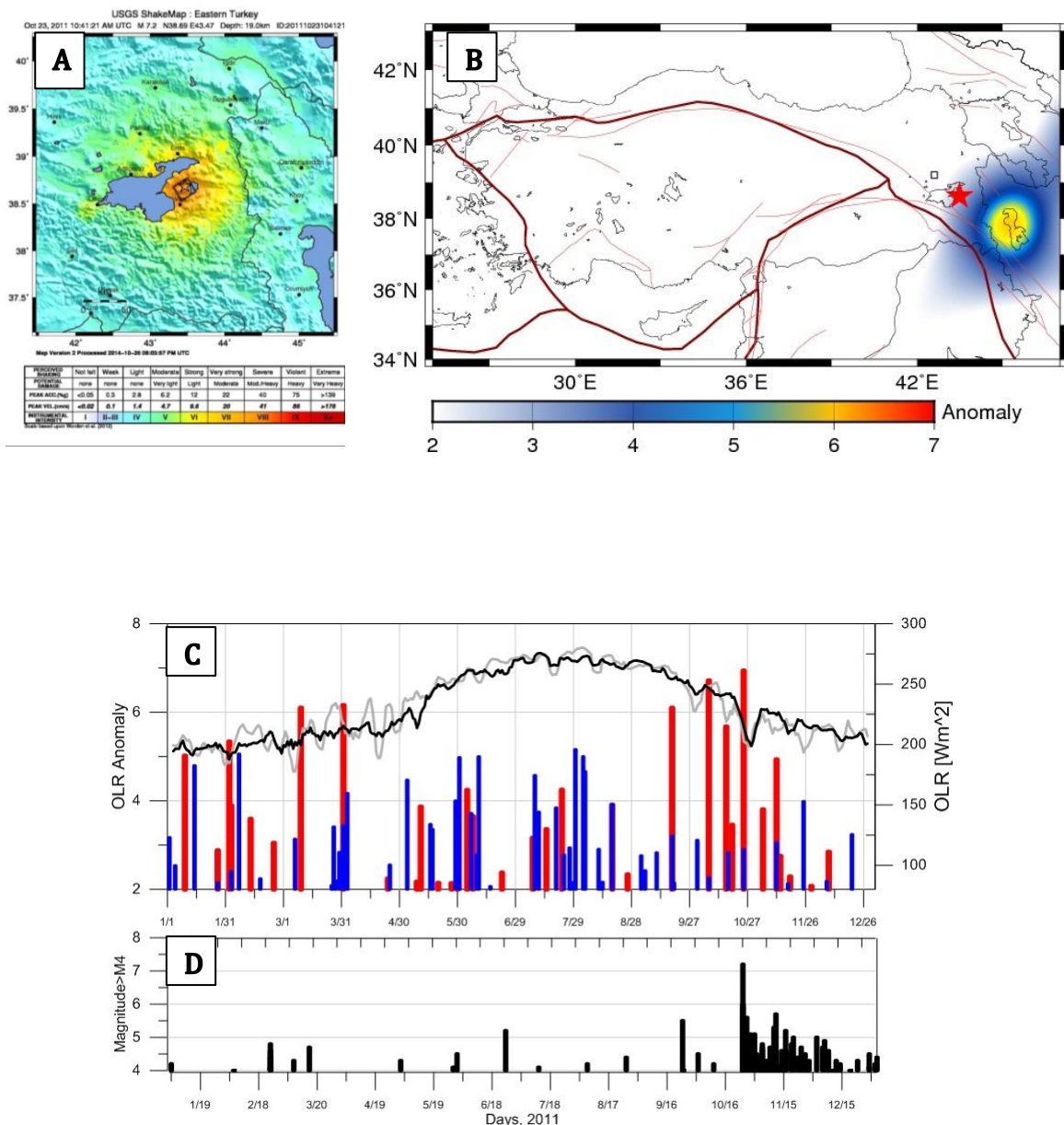
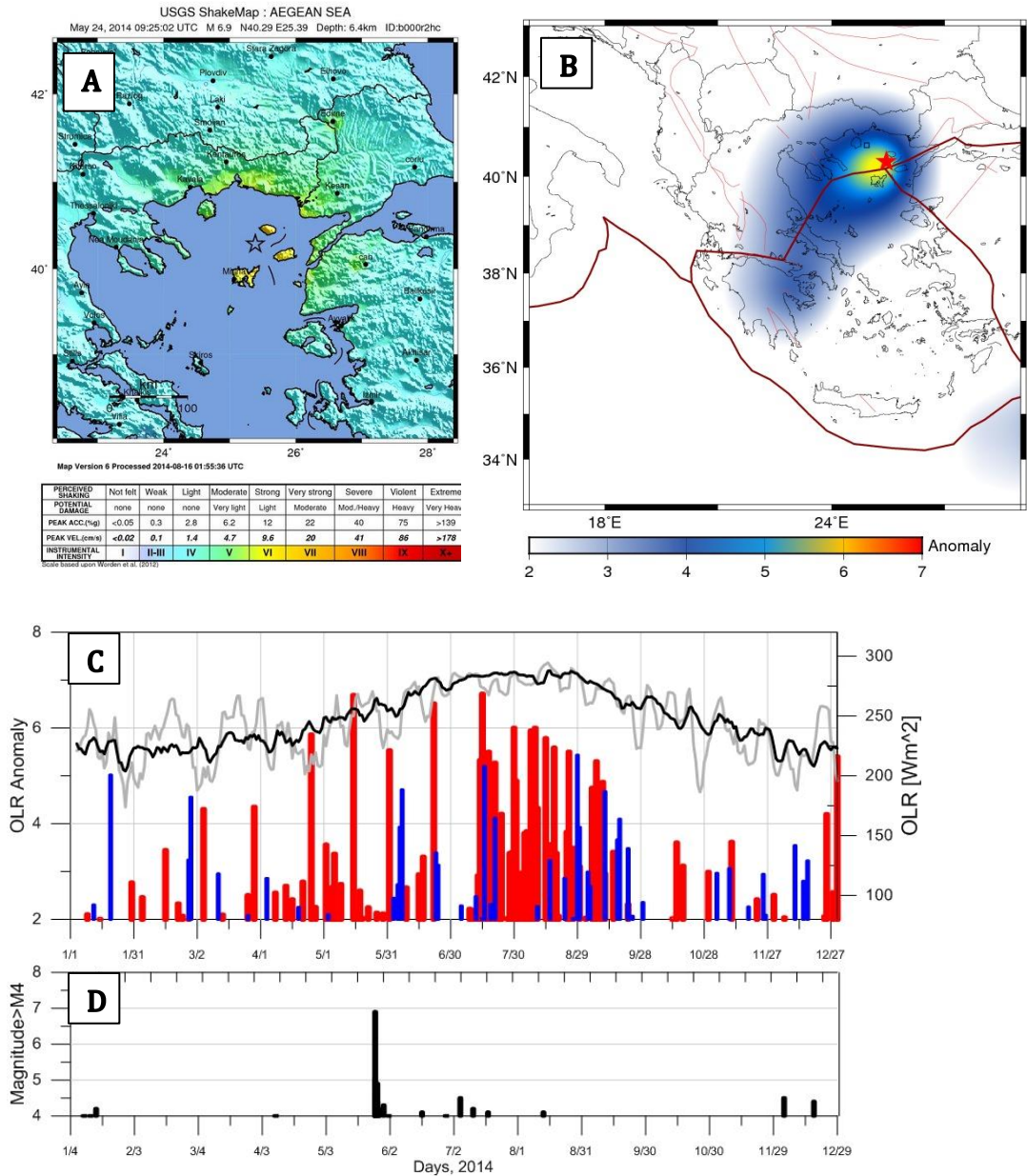


Figure 3. TRA associated with M7.3 of Oct 23, 2011, Van, Turkey; A. USGS shake map (top left), B. Nighttime TRA anomalous maps observed on Oct 19th, 2011, 4 days in advance. Epicenter is marked with red star, tectonic plate boundaries with red line, and major faults with brown color (top, right). C. Yearly time series of nighttime OLR over the epicentral area, anomalous values (red), 2011 mean value OLR (gray), 2006-2011 mean value (black), 2010 anomalous trend (blue) with no major seismicity for comparison. D. 2011 seismicity (EMSC catalog) M>4 near the epicentral area (bottom, black)

The continuous satellite monitoring of OLR data over Greece obtained from NOAA POES satellite system showed rapid increase during the middle of April 2015 and they indicated a probable large earthquake preparation process in Aegean Sea (Fig. 4). A strong anomaly in the atmosphere was detected (prospectively) at 19:00 LT on May 14, 2015 with 2.5 sigma significance over 25 years of data analysis (Ouzounov et al, 2015). On May 24, 2015, after the anomaly was detected a M6.9 earthquake occurred in the area of the observed atmospheric anomaly.



375
376
377
378
379
380
381
382
383
384
385
386
387
388
389
390
391
392
393
394
395
396
397
398
399
400
401
402
403
404
405
406
407
408
409
410

Figure 4. TRA associated with M6.9, May 24, 2014, earthquake in the Aegean Sea. A./USGS shake map (top left), B. Nighttime TRA anomaly map observed on May 14, 2015, 10 days in advance. Epicenter is marked with red star, tectonic plate boundaries with red line, and major faults with brown color (top, right) .C Yearly time series of night time OLR over the epicentral area, anomalous values (red), 2014 mean OLR (gray), 2006-2041 mean value (black), 2013 anomalous trend (blue) with no major seismicity for comparison D. Seismicity (EMSC) $M > 4$ near the epicentral area (bottom, black).

During end of July and firing the August 2014 we detected (prospectively) a large TRA anomaly transient field over Northern California (Fig. 5). The location was shifted north West by about 100 km from the M6.0 of Aug 24rd epicentral area. For this particular case we used a hybrid OLR product between NOAA AVHRR and EOS AIRS observations to advance the temporal coverage of the San Francisco area. In the Southern Napa Valley, California earthquake the value of the OLR compared to the reference field of August 2004 to 2014, indicated a rapid change in the thermals anomalous flux rate at 7:00 on August 23. The registered anomalous pattern was the largest energy flux anomaly over the California at this time. (Ouzounov et al., 2014)

411
412
413
414
415
416
417
418
419
420
421
422
423
424
425
426
427
428
429
430
431
432
433
434
435
436
437
438
439
440
441
442
443
444
445
446
447
448
449
450
451
452
453
454
455
456
457
458
459
460
461
462
463
464
465
466
467

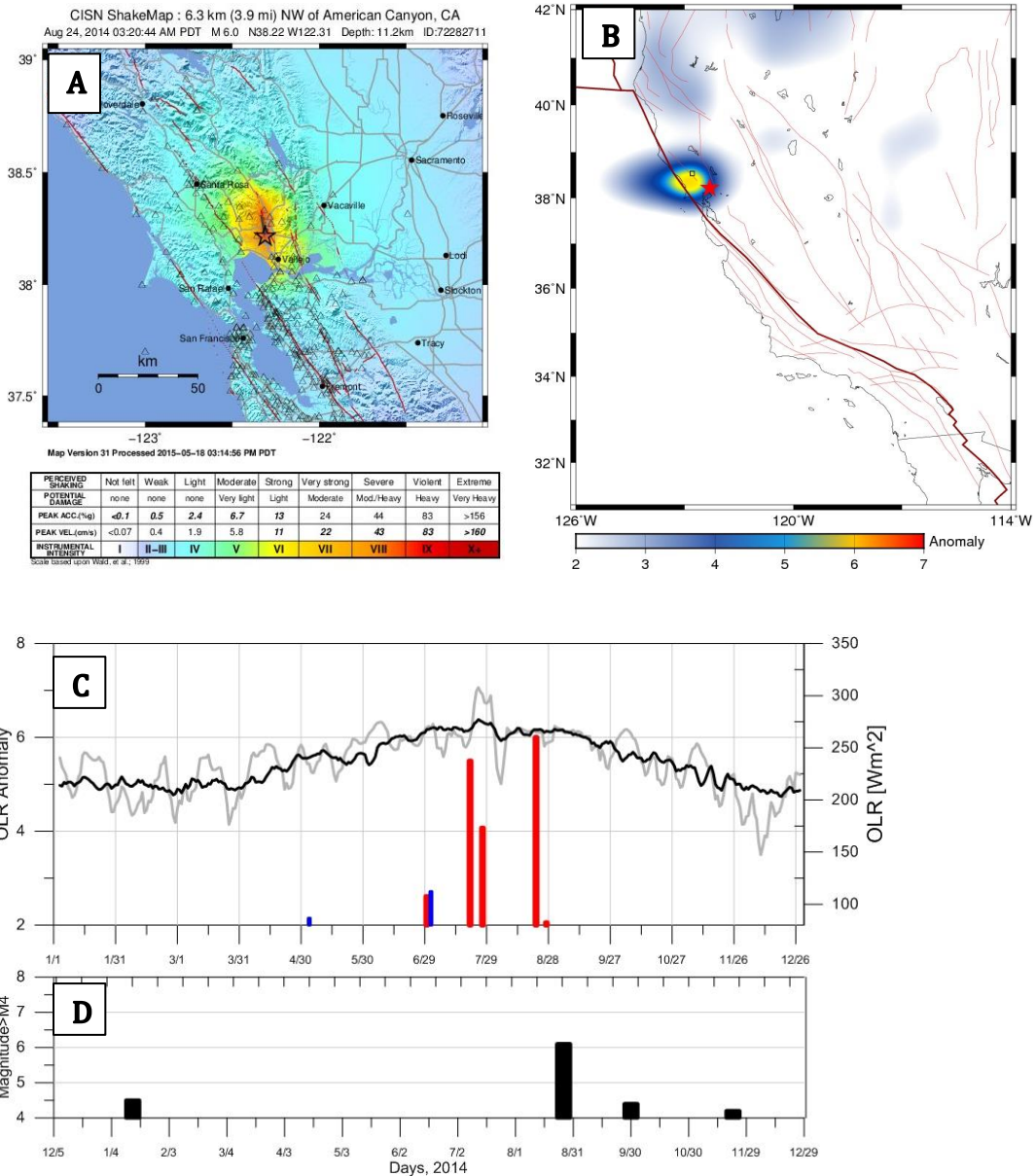


Figure 5. TRA associated with M6 Aug 24, 2014, Napa Valley, California; A./USGS shake map (top left), B. Nighttime TRA anomaly map observed on Aug 22nd 2014, 2 days in advance. Epicenter is marked with red star, tectonic plate boundaries with red line, and major faults with brown color (top, right). C Yearly time series of night time OLR over the epicentral area: anomalous values (red), 2014 mean value OLR (gray), 2006-2014 mean value (black), 2013 anomalous trend (blue) with no major seismicity for comparison. D. 2014 seismicity (EMSC) $M > 4$ near the epicentral area (bottom, black)

The daily OLR variations (OLR anomalous values ≤ 2) are caused by the daily environmental variations in the vertical atmospheric circulations in middle atmosphere. The significant deviation from the normal state for Van case started September 15, reached a maximum value (OLR,7) on October 22 and went back to normal state on December 15, 2011 (Fig.3). For 2014 Aegean Sea event the breakout started in the beginning of February, the anomaly reached a maximum around May 14 and came back to normal on October 15, 2014 (Fig.5). For South Napa the break started in July 20 with a systematic increase reaching the maximum level (OLR values are around 7) in the OLR acceleration on August 22 and going back the normal state in mid-September 2014 (Fig.5).

At the ending of the event the anomalous pattern coincided with the same period as the ending of the major aftershock activities in all of the cases. To test the significance of the results for confutation – i.e. absence of anomalous OLR signals in absence of major

468 seismic events (Tramutoli et al, 2005), we calculated the OLR anomalies for the same
469 location for one full year before the major event. The yearly time distribution of OLR
470 shows significant lower level (Fig, 3,4, and 5 with blue columns) with a randomly
471 distributed pattern. Thus it is not reproducing the strength and temporal evolution of the
472 OLR anomalous signals generated during the year (Fig, 3,4,and 5 with red columns). The
473 pre-earthquake OLR anomalies for M7.0 Van (Fig. 3) and M6.9 Greece (Fig. 4) are not
474 overlapping in time with the maxima of the seasonal variations of OLR usually higher
475 during June-August in the Northern Hemisphere (Fig 3.4, black color curve), which is an
476 indication for the non-weather related origin of OLR anomalous values and their primarily
477 connection with the geodynamics. The M6.0 South Napa occurred in the middle of the
478 summer, 2014 (August 24) and shows that the computational approach used can rival an
479 anomalous pattern even during a period of natural enchantment of the background
480 radiation field (Fig 5). Analogous findings were observed within a few days prior to the
481 most recent major earthquakes in Japan (M9, Tohoku, 2011), China (M7.9, Wenchuan
482 2008), Italy (M6.3, L'Aquila 2009), Samoa (M7, 2009), Haiti (M7, 2010) and Chile
483 (M8.8, 2015) (Ouzounov et al., 2015ab; Pulinets et al., 2015).

484 **3. Thermal energy associated with some large earthquakes**

485 We have examined the different energy components of recent strong earthquakes ($M > 8$),
486 using observations and theory. Our motivation is to explore the physics of the associated
487 thermal phenomena, *i.e.* to compare the energy of the earthquakes, as well as the latent
488 heat released prior to the events. We have examined the energy budget of earthquakes via
489 theory and observations for the three mega quakes of Sumatra, M9.1, 26 December 2004;
490 M8.7, 28 March 2005; and M9.0, Tohoku, 2011 and evaluated mechanical and thermal
491 energies. In other words, we evaluated the thermal energy, required to create the energy
492 budget associated with these large quakes (Pulinets et al., 2006a, 2006b, Kafatos et al.,
493 2010). Space-based observations and model outputs can be used for pre-seismic energy.
494 We expect that our analysis will shed light on underlying physics (such as of our proposed
495 pre-earthquake lithosphere/ atmosphere/ interaction) associated with some of the largest
496 earthquakes and would potentially be useful for warning of future events. It is large events
497 that give us information about the total energetics and, therefore, they are very useful to
498 provide information about the underlying physics.

499 For the seismic moment M_0 , one can use the rupture length, the rupture width and the slip
500 to obtain values of 8.9×10^{22} J, 1×10^{22} J and 3.2×10^{22} J for the 26 Dec. 2004, the 28
501 March 2005, and 11 March 2011 events, respectively. We calculated that $2,000 \text{ km}^3$ land
502 mass was displaced in the 26 Dec. 2004 Sumatra earthquake, while $1,300 \text{ km}^3$ of land
503 mass was displaced in Japan. The seismic moment can be considered to be the total energy
504 in the pre-quake stressed configuration, and is essentially an estimate of the total available
505 energy budget. It is also close to estimate of change in gravitational potential energy Mgh ,
506 where M is the mass of the plate, g is gravitational acceleration, and h is the vertical
507 distance the plate is displaced. The original Richter energy was supposed to refer to local
508 damage near the epicenter. But the available energies are much higher than energies
509 creating havoc at the surface. We are estimating the energies of seismic moment, latent
510 heat and moving of landmasses. It is not surprising then that mega quakes of magnitude 9
511 seem to affect the entire Earth. We can estimate the change in the rotational energy of the
512 Earth for these large events as, for example, the rotational rotation period of the Earth
513 decreased 2.68 microseconds while the oblateness decreased by 1 part in 10^{10} for the main
514 Sumatra event (Gretchen, 2005).

515 We compared the latent heat (LH) energy, obtained by integrating (SLHF) over the area
516 and the time of the earthquake, accounting for the overall thermal and mechanical
517 associated energies. The SLHF data used are taken from NCEP/NCAR dataset maintained
518 at the International Research Institute on Climate Prediction (IRI) (<http://iri.columbia.edu>).
519 Thermal outgoing long wave radiation (OLR) data can also be used.

520
521
522
523
524
525
526

We compared the magnitudes of the energies associated with the 9.3, 8.7 and 9.0 events and their accompanying phenomena. Using the usual conversion of magnitudes to energy (Bath, 1996) associated with surface waves, $E_Q \sim 4.5 \times 10^{18} \text{ J}$, $E_Q \sim 5.5 \times 10^{17} \text{ J}$, and $1.5 \times 10^{18} \text{ J}$ respectively. The total energy release of the entire series of earthquakes, including the many aftershocks, is dominated by these three events. The latent heat energy released prior to the earthquake, E_{LH} , can be estimated by:

527

$$DSLHF(\mathbf{r}) = \sum_{i=1}^{N-1} \frac{SLHF(r)}{N-1} \quad (4)$$

528

where \mathbf{r} is taken in practice by summing pixel by pixel (\mathbf{r}) and integrating over time. The result is insensitive because of the strongly peaked nature of the signal occurred around 7 Dec., 2004, 19 days in advance of the 26 December 2004, Sumatra earthquake (Cervone et al, 2004); and similarly on March 3-10, associated with Tohoku earthquake (Ouzounov et al., 2011). The total LH associated with the three main events are $E_{LH} \sim 8.0 \times 10^{18} \text{ J}$, $3.1 \times 10^{19} \text{ J}$ and $1.9 \times 10^{19} \text{ J}$ associated the 28 March 2005, 26 Dec. 2004 and 11 March 2011 earthquakes respectively, (See Table 2).

529
530
531
532
533
534
535
536
537

	Events	M_w	E_Q Richter $\times 10^{17} \text{ J}$	Rupture length	LH energy $\times 10^{18} \text{ J}$	SLHF, Wm^2	SLHF Durations
1	12.26.2004, Sumatra	9.1– 9.3	420	~1500km	~310	100	10 days
2	03. 28.2005, Sumatra	8.7	5.7	~300km	~8	80	5 days
3	03.11. 2011, Japan	9.0	150	~500km	~190	90	8 days

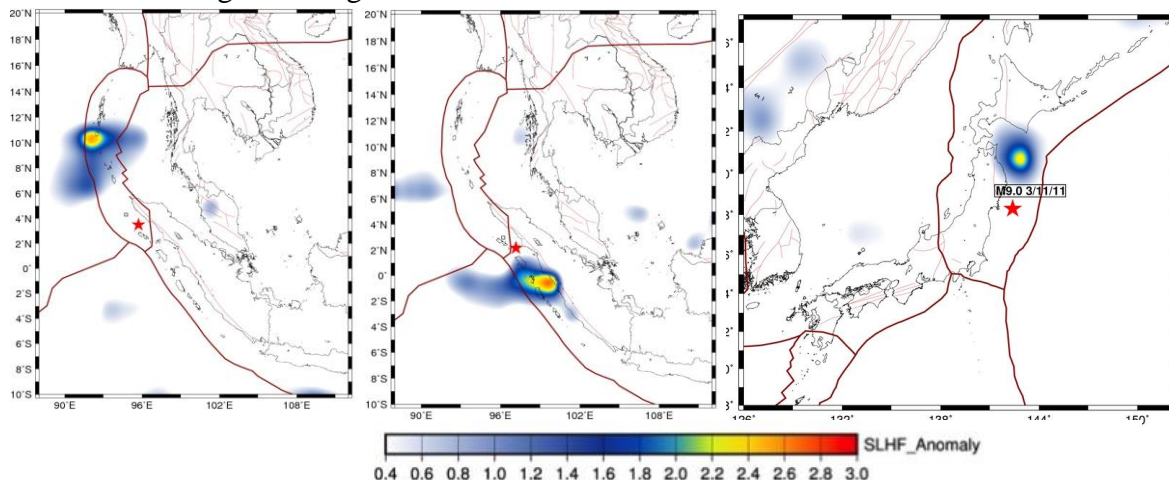
538
539
540

Table 2 Energies comparison for the major earthquakes in Sumatra 2004, 2005 and Tohoku 2011, Japan

541

The above energy values give us the main energy channels involved.. It would be important to research the interconnection between the mechanical processes and their energies, including the latent heat, and associated thermal energies (see below), which might be observed as surrogates for the total energies involved in earthquakes. The poorly resolved global energies may very well turn out to be the dominant term is the latent heat energy release, $> \sim 3 \times 10^{19} \text{ J}$, as we are observing LH, released through the ocean, while the mechanical/kinetic energies are an order of magnitude or less and the energy of rupture an order of magnitude higher.

550
551
552
553
554
555
556
557
558
559
560
561



562
563
564
565 *Figure 6. Anomalous daily maps of SLHF a/. Dec 15, 21004, eleven days before M9.3 of Dec 26*
566 *Sumatra 2004; b/.March 6, 2005, twenty days before Sumatra 2005; c/.March 5, 2011, six days*
567 *before Tohoku 2011. Epicentres are marked with red star, tectonic plate boundaries with red line,*
568 *and major faults with brown colour.*
569

570 Our analysis shows that latent heat has been detected several days prior to the earthquake.
571 On Dec 15, 2004, eleven days before the M9.3 Sumatra earthquake a strong anomaly was
572 observed along the rupture zone north of the site of the future epicenter, with a value >4
573 sigma (Fig. 6a). Similar phenomena with lower intensity and spatial extension were
574 observed on March 6, 2005, twenty days before the March 26, 2005 M8.6 earthquake (Fig.
575 6b). For the 2011 Tohoku a similar pattern occurred, on March 5, only 6 days before the
576 main shock, strong SLHF anomaly was observed north of the epicentral area, along the
577 future rupture zone (Fig. 6c). As such, the overall earthquake phenomenon apparently
578 causes LH release; suggesting that terrestrial internal energy is used to produce
579 evaporation. The change in internal energy on a short timescale such as the December
580 2004, M9.3 earthquake in Sumatra, March 2005 for M8.6 and March 2011 for M9.0 in
581 Tohoku, We found that the ratios of the seismic moment; and the change of mechanical
582 energy, to latent heat, is also a function of the size of the rupture, indicating latent heat is a
583 direct surrogate of the total geophysical energies involved.
584

585 **4. Thermal anomalies and the Lithosphere-Atmosphere coupling**

586 Several processes have been considered as possible contributors to the transient short-
587 lived “thermal anomalies”: (a) rising fluids that would lead to the emanation of warm
588 gases (Salman et al., 1992; Gorny et al., 1988); (b) rising well water levels and CO₂
589 spreading laterally and causing a “local greenhouse” effect (Qiang et al., 1991; Tronin et
590 al., 2002; Tramutoli et al., 2005); (c) activating positive-hole pairs during rock
591 deformation (Freund, 2002); (d) frictional heat around the active fault (Tagami et al.,
592 2008); and (e) air ionization by radon and latent heat change due to change of air humidity
593 (Pulinets and Ouzounov 2011).

594 TIR anomalies observed from satellites and associated with earthquake processes are less
595 likely to be the result of: (i) earth crust heat flow (because of short-lived phenomena); (ii)
596 convective transport as result of friction processes associated with active faulting (because
597 of their rapid build- up); or (iii) meteorological origin (because of the long persistence of
598 TIR over the same region). The most probable cause of the physical mechanism of the
599 thermal anomaly generation can be the morphology and the release of thermal energy
600 estimations. The most important one is that thermal anomalies are observed over both the
601 land and the ocean. Only strong gas discharges (including the underwater gas discharges),
602 as described by Khilyuk et al. (2000), could be a potential candidate for this possible
603 mechanism.

604 Although their detailed underlying mechanisms are still under debate (*e.g.* Freund, 2011;
605 Pulinets and Ouzounov, 2011), in the case of earthquakes, the general process that could
606 affect the atmosphere and ionosphere "from below" might be the generation of TRA and
607 the penetration of anomalous electric fields originating close to the surface extending into
608 the ionosphere (Kuo et al., 2011). It was instrumentally documented that the latest stage of
609 the earthquake cycle (Dobrovolsky *et al.*, 1979) is characterized by mechanical changes in
610 the Earth's crust accompanied by geochemical and electromagnetic anomalies (Scholz *et*
611 *al.*, 1973; Kasahara, 1981). The link between the crustal transformation under loading and
612 asperities on faults has been studied (Schorlemmer et al., 2004). The formation of
613 asperities, increasing crustal porosity this leads to changes in gas migration evidently by
614 an increase of gas release into the boundary layer of the atmosphere.

615 At the last stage of earthquake preparation we observe the activation of faults within the

616 area of the earthquake within this area that leads to increased emanation of gases such as
617 carbon dioxide, methane, hydrogen, helium, including radon (Step #1, Fig.7). It was
618 established that together with radon diffusion within the crust it is actively released in the
619 atmosphere by carrier gases, which usually are carbon dioxide and methane. A correlation
620 was established between the deformations and radon release (Aumento, 2002). Radon, due
621 to its radioactivity, produces the air ionization (Harrison et al., 2010) (Step #2, Fig.7).
622 Air ionization accelerates, drastically, the formation of cluster ions due to newly formed
623 ion hydration. This process is called Ion Induced Nucleation (IIN) (Laakso et al., 2002).
624 (Step #3, Fig.7). This process leads to formation of large charged ion clusters consisting
625 of the charged core ion with the envelope of water molecules, which attach to the ions due
626 their high dipole moment (Sekimoto and Takayama, 2007). IIN is essentially nonlinear
627 process because it is catalytic exothermic process with simultaneously coexisting two
628 aggregation phase states of the water: condensed and vapor.
629 We will discuss the key question in relationship between the generation of TRA in the
630 atmosphere and the pre-earthquake process. The question is *-What are the drivers*
631 *producing a strong modification of the atmosphere?* There is a paradox between the
632 catalytic process: and the energy release, but the source of the energy is different. In the
633 case of TRA it is the latent heat of the water vapor in the air. Here are some estimates:
634 The latent heat constant is $Q = 40.683 \text{ kJ/mol}$, it means that the heat released per one
635 molecule is $U_0 = Q/N_A = 0.422 \text{ eV}$ where $N_A = 6.022 \cdot 10^{23} \text{ 1/mol}$ (Avogadro number).
636 Ionization effectiveness depends on the number of water molecules attached to the ion. If
637 the particle grows to some value of m_{max} , the number of energy release will be: $w =$
638 $m_{\text{max}} U_0$. If the ion production rate is dN/dt , the heat released in the atmosphere could be
639 expressed as $P_a = w \cdot dN/dt$. Experimentally the clusters of the order of 1000 nm were
640 found (Pulinets and Ouzounov, 2011). To ionize any air molecules we need the energy of
641 10-15 eV. One particle of 1000 nm size contains $0.4 \cdot 10^{12}$ water molecules this produces
642 the heat release $0.422 \text{ eV} \times 0.4 \cdot 10^{12} = 1.7 \cdot 10^{11} \text{ eV}$. So one can easily see that the
643 energy gain due to the latent heat release is $1.7 \cdot 10^{11} / 15 = \sim 10^{10}$. This is the essential
644 value - *Radon and ionization does not produce any energy, the energy is released due to*
645 *condensation of the water vapor on ions, and consequent release of the latent heat*
646 *contained in the air water vapor.*

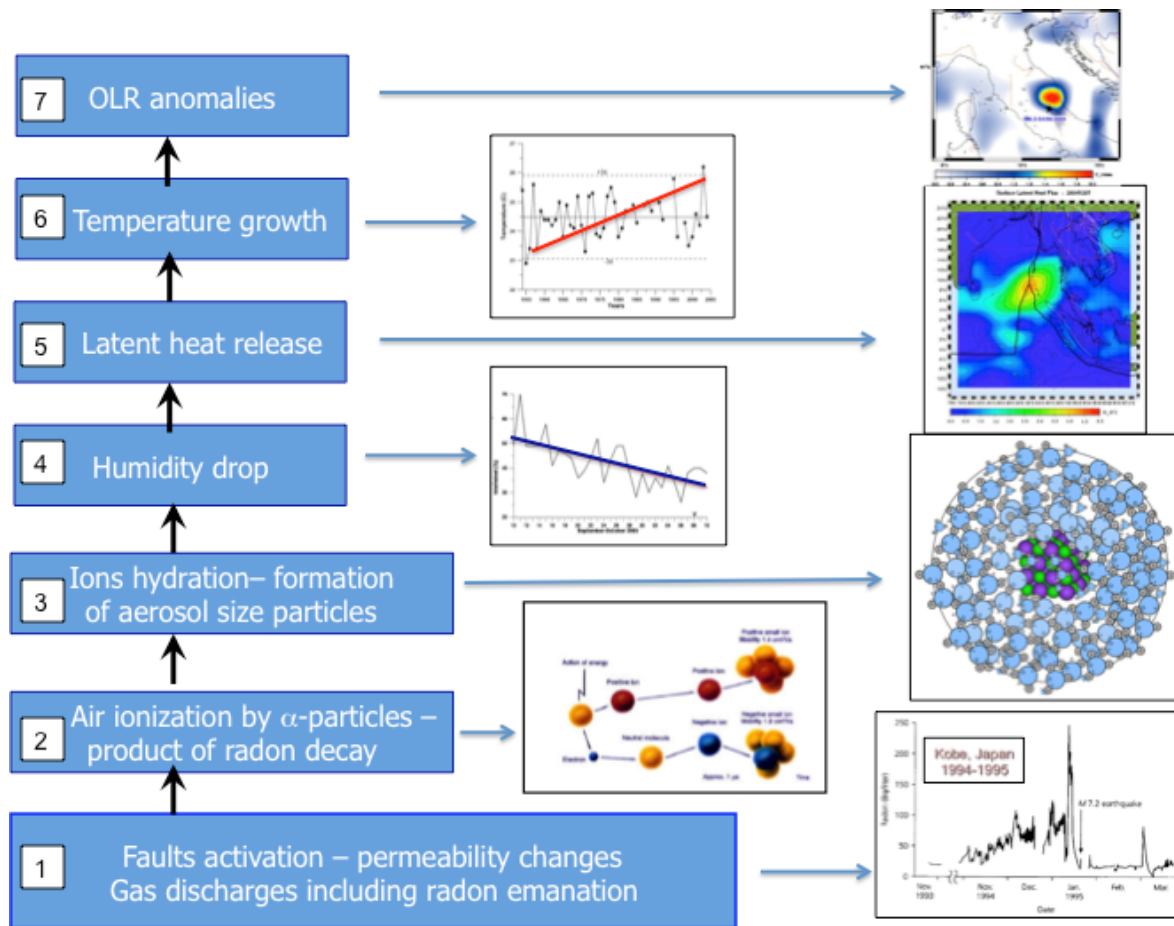


Figure 7. Principle Flow-chart of the TRA generation (Pulinets and Ouzounov, 2011)

647
648
649
650
651 In Fig.7 we can now explain rectangles Step #4 (relative air humidity drop because of
652 water vapor condensations on ions), Step #5 (the latent heat release) and Step #6 (air
653 temperature growth). It is well known from meteorology that sharp drops of humidity are
654 accompanied by air temperature growth. Because of the general atmospheric circulation
655 the additional heat flux release due to the latent heat release could be registered in the long
656 wave part of the infrared emission within the transparency window of the atmosphere 8-12
657 μm from satellites (so called outgoing Longwave radiation – OLR), (step #7 Fig. 7). *What*
658 *is amount of outgoing energy flux we should expect at TOA as Outgoing Longwave*
659 *Radiation flux was shown in Fig. 1? Each α -particle emitted by ^{222}Rn with the average*
660 *energy of $E_{\alpha}=5.46$ MeV can produce $\sim 3 \cdot 10^5$ electron-ion pairs. From the real observation*
661 *of radon activity, before an earthquake the level could be ~ 2000 Bq/m 3 (Inan et al.,*
662 *2008). The ion production rate of Rn is $\sim 6 \cdot 10^8$ s $^{-1}$. We already show from our last*
663 *estimation that the particle 1000 nm size contains $0.4 \cdot 10^{12}$ water molecules. During the*
664 *water vapor condensation process the latent heat release is $U_0 \sim 40.68 \cdot 10^3$ J/mol (1 mol*
665 *= $6.022 \cdot 10^{23}$). That means that the given radon activity with formation of particles of 1000*
666 *nm size gives the thermal energy output of 16 W/m 2 . That is exactly the range of*
667 *~ 20 W/m 2 we were able to observe as TRA anomalies at TOA by using NOAA/AVHRR*
668 *data (Ouzounov et al, 2007). There are two main consequences of the IIN process: (1)*
669 *latent heat release due to water vapor condensation on ions; and (2) changes of the air*
670 *conductivity leading to the local changes in the Global Electric Circuit – for the*
671 *electromagnetic coupling of the atmosphere and ionosphere. The chain of these physical*
672 *processes has been proposed as an essential part of the Lithosphere-Atmosphere-*
673 *Ionosphere-Magnetosphere Coupling concept. (Pulinets and Ouzounov, 2011, Pulinets et*
674 *al., 2015). The presence of thermal infrared anomalies (TIR) at different levels (ground*
675 *level, troposphere, tropopause) and space plasma anomalies including the GPS/TEC,*

676 allow us to register them from space using a multi-parameter approach (Ouzounov et al,
677 2011)

679 **5. Summary and Conclusions**

680 Our results show that several days before some earthquakes (Figs. 3,4,5) infrared signals
681 related to earthquake processes were observed near the epicentral areas by the NOAA
682 POES satellite as OLR hotspots. The OLR hot spots appeared quickly, stayed over the
683 same regions from several hours or up to few days, and then disappear rapidly. The time
684 lag for the M7.3 earthquake in Van, Turkey was 4 days; for the M6.9 earthquakes in
685 Aegean Sea, Greece was 10 day and for M6.0 earthquake in California was 2 days. This
686 enhancement of OLR could be explained as a result of water vapor condensation on ions,
687 with a large amount of latent heat being released. The initial process involves an
688 ionization of the near-ground layer due to an increased concentration of gasses (including
689 radon) emitted from active tectonic faults (Pulinets and Ouzounov, 2011). The transient
690 nature in radiative emission preceding large earthquakes follows a general temporal-
691 spatial evolution pattern, which is similar to other large earthquakes worldwide (Kuo,
692 2011 and Ouzounov et al., 2016). The transitional OLR anomalous data usually varied
693 between 16-21 W/m². They are residuals derived from the daily mean OLR compared with
694 the background field. The latter was derived from multiple years of observations, over the
695 same location and local time, and normalized by the standard deviation (Ouzounov et al,
696 2007, 2011). From space-born observations of atmospheric conditions, we have shown the
697 consistent occurrence of TRA anomalies at the TOA, over the region of maximum stress
698 associated with, and preceding, large earthquakes. Because of their relatively long
699 duration, these anomalies do not appear to be of meteorological origin. We evaluated the
700 mechanical and thermal energies of three major earthquakes to explore the physics of
701 associated thermal phenomena. Our estimates show that the LH released prior to the
702 events is larger than the seismic energy released during the quake. We show that in large
703 earthquakes the associated phenomena may stand out energetically with measurements
704 above variance that arises from other geophysical processes. As we have a greater energy
705 budget for these large events, we emphasize that it can be used to establish a more general
706 earthquake energy phenomenology. Our analysis of transitional thermal fields of recent
707 major earthquakes (M7.3 Van, Turkey, 2011; M6.9 Aegean sea, Greece, 2014; and M6.0
708 Napa Valley, California, 2014) has demonstrated the presence of correlated variations of
709 TRA anomalies in the atmosphere, implying their connection with pre-earthquake
710 processes. Our results suggest the existence of an atmospheric response triggered by the
711 coupling processes between the lithosphere and atmosphere.

712 **ACKNOWLEDGMENTS**

713 The authors thank to the NOAA's Climate Prediction Center (USA), NASA Goddard
714 Earth Science Center (GES DAAC) for OLR data and to International Research Institute
715 for Climate and Society for SLHF data. Special thanks to USGS and EMSC for providing
716 earthquake information services and data. Dimitar Ouzounov gives thanks to all his
717 graduate students from NASA DEVELOP National program at Goddard SFC and
718 Chapman University for helping in the processing of satellite data. Dimitar Ouzounov and
719 Sergey Pulinets thank the International Space Science Institute (Bern and Beijing) for
720 support of the team "Validation of Lithosphere-Atmosphere-Ionosphere-Magnetosphere
721 Coupling (LAIMC) as a concept for geospheres interaction by utilizing space-borne multi-
722 instrument observations". Menas Kafatos thanks Kent S. Wood for useful input in the
723 energetics involved.

Reference

- Aumento, F. (2002), Radon tides on an active volcanic island: Terceira, Azores, *Geofísica Internacional*, 41,4,p. 499–505.
- Bath, M., (1966), Body wave energy from seismograms. In:L.H. Ahrens et al. (Editors), *Physics and Chemistry of the Earth*. Pergamon Press, London, 7: 133-137.
- Bryant, N., Zobrist, A., Logan, T., (2003), Automatic co-registration of space-based sensors for precision change detection and analysis. *IGARSS 2003 Transactions*. France, 7. 21–26
- Carreno, E., Capote, R., Yague, A., (2001) Observations of thermal anomaly associated to seismic activity from remote sensing. General Assembly of European Seismology Commission, Portugal, 10–15 September, 265–269.
- Cervone, G., Kafatos, M., Napolitano, D., Singh, R.P., (2004) ,Wavelet maxima curves of surface latent heat flux associated with two recent Greek earthquakes, *Natural Hazards and Earth System Sciences*, VL 4,IS 3, 359-374
- Cervone, G., Maekawa, S., Singh, R.P., Hayakawa, M., Kafatos, M., and Shvets, A., (2006), Surface latent heat flux and nighttime LF anomalies prior to the Mw=8.3 Tokachi-Oki earthquake, *Nat. Hazards Earth Syst.*
- Dey, S., Sarkar, S., Singh, R.P., (2004), Anomalous changes in column water vapor after Gujarat earthquake. *Advances in Space Research* 33 (3), 274–278
- Di Bello, G., Filizzola, C., Lacava, T., Marchese, F., Pergola, N., Pietrapertosa, C., Piscitelli, S., Scaffidi, I., Tramutoli, V. (2004) Robust. satellite techniques for volcanic and seismic hazards monitoring. *Annals Geophys.* 47 (1), 49–64
- Dobrovolsky, I. R., S. I. Zubkov, and V.I. Myachkin, (1979) ,Estimation of the size of earthquake preparation zones, *Pageoph.*, 1025 -1044
- Filizzola C., Pergola N., Pietrapertosa C., Tramutoli V. (2004), Robust satellite techniques for seismically active areas monitoring: a sensitivity analysis on September 7th 1999 Athens's earthquake. *Physics and Chemistry of the Earth*, 29, 517-527.
- Fisher, S., K. Sulia, D. Ouzounov, F. Policelli, and M. Ferrucci (2008), Data Exploration of Atmospheric Thermal Signals over Regions of Tectonic Faulting and Earthquake Processes, *AGU Fall Meeting Abstracts*
- Freund, F., (2002), Charge generation and propagation in rocks, *J.Geodynamics* 33, 545–572
- Freund, F. (2011), Pre-earthquake signals: Underlying physical processes, *J. of Asian Earth Sci.*, 41, 383–400
- Genzano N., Aliano C., Filizzola C., Pergola N., Tramutoli V. (2007), A robust satellite technique for monitoring seismically active areas: the case of Bhuj - Gujarat earthquake. *Tectonophysics*, 431, 197-210
- Genzano, N., Aliano, C., Corrado, R., Filizzola, C., Lisi, M., Mazzeo, G., Paciello, R., Pergola, N., Tramutoli, V. (2009), RST analysis of MSG-SEVIRI TIR radiances at the time of the Abruzzo April 6th 2009 earthquake. *Natural Hazards and Earth System Sciences* - vol. 9, pp. 2073-2084.
- Goosse H., P.Y. Barriat, W. Lefebvre, M.F. Loutre and V. Zunz, (2016). Introduction to climate dynamics and climate modeling. Online textbook available at <http://www.elic.ucl.ac.be/textbook>.
- Gorny, V.I., Salman, A.G., Tronin, A.A., Shilin, B.B., (1988), The Earth outgoing IR radiation as an indicator of seismic activity. *Proceeding of the Academy of Sciences of the USSR*, 301: 67.
- Gretchen Cook-Anderson, Dolores Beasley, (2005) NASA Details Earthquake Effects on the Earth. *NASA* (press release). *January 10, 2005*
- Gruber, A. and Krueger, A., (1984), The status of the NOAA outgoing longwave radiation dataset. *Bulletin of the American Meteorological Society* ,65, 958–962
- Han, P., Hattori, K., Hirokawa, M., Zhuang, J., Chen, C.H., Febriani, F., Yamaguchi, H.,

- 776 Yoshino, C., Liu, J.Y., Yoshida, S., (2014) Statistical analysis of ULF
777 seismomagnetic phenomena at Kakioka, Japan, during 2001-2010. *Journal of*
778 *Geophysical Research: Space Physics* 119, 4998–5011.
- 779 Han, P., Hattori, K., Huang, Q., Hirooka, S., Yoshino, C., (2016) Spatiotemporal
780 characteristics of the geomagnetic diurnal variation anomalies prior to the 2011
781 Tohoku earthquake (Mw 9.0) and the possible coupling of multiple pre-
782 earthquake phenomena. *Journal of Asian Earth Sciences* 129, 13–21.
- 783 Hayakawa, M. (1999), *Atmospheric and Ionospheric Electromagnetic Phenomena with*
784 *Earthquakes*, Terra Sci. Pub. Co., Tokyo.
- 785 Hayakawa, M. and O. A. Molchanov (2002), *Seismo Electromagnetics, Lithospheric-*
786 *Atmospheric- Ionospheric coupling*, Terra Sci. Pub. Co., Tokyo.
- 787 Hayakawa, M (Editor), (2012), *Frontier of Earthquake short-term prediction study*,
788 Nihon-Senmontosho, Japan, 794p
- 789 Harrison R.G., Aplin K.L., Rycroft M.J. (2010) Atmospheric electricity coupling between
790 earthquake regions and the ionosphere, *JASTP*, 72, 376–381, 2010
- 791 Inan S, Akgu T, Seyis C, Saatc R, Baykut S, Ergintav S and Bas M (2008).
792 Geochemical monitoring in the Marmara region (NW Turkey): A search for
793 precursors of seismic activity. *J Geophys Res* **113**: B03401,
794 doi:10.1029/2007JB005206.
- 795 Kafatos, M., D. Ouzounov, S. Pulnests, K. Hattori, J. Liu, M. Parrot, and P. Taylor ,
796 (2010), Multi Sensor Approach of Validating Atmospheric Signals Associated
797 with Major Earthquakes, EGU General Assembly Conference Abstracts 12,
798 1418
- 799 Kasahara, K., (1981) *Earthquake Mechanics*, Cambridge University Press, Cambridge, 1-
800 248,
- 801 Kuo, C.L., Huba, J.D., Joyce, G., Lee, L.C. (2011) Ionosphere plasma bubbles and density
802 variations induced by pre-earthquake rock currents and associated surface
803 charges. *Journal of Geophysical Research*, 116, 1029-1039
- 804 Kon, S., M. Nishihashi, and K. Hattori (2010), Ionospheric anomalies possibly associated
805 with $M \geq 6$ earthquakes in Japan during 1998-2010: Case studies and statistical
806 study, *J. Asian Earth Sci.*, **41(4)**:410-420, DOI: 10.1016/j.jseas.2010.10.005
- 807 Laakso L, Mäkelä JM, Pirjola L, Kulmala M (2002), Model studies on ion-induced
808 nucleation in the atmosphere. *J. Geophys. Res.*, 107(D20): 4427,
809 doi:10.1029/2002JD002140
- 810 Liebmann B. and C.A. Smith, (1996), Description of a Complete (Interpolated) Outgoing
811 Longwave Radiation Dataset. *Bulletin of the American Meteorological Society*,
812 77, 1275-1277.
- 813 Lisi M., Filizzola C., Genzano N., Grimaldi C. S. L., Lacava T., Marchese F., Mazzeo G.,
814 Pergola N. and Tramutoli V (2010) A study on the Abruzzo 6 April 2009
815 earthquake by applying the RST approach to 15 years of AVHRR TIR
816 observations. *Natural Hazards and Earth System Sciences*, 10, pp. 395–406.
- 817 Liu, D., Kang, C., (1999) Thermal omens before earthquakes. *ACTA Seismologica*
818 *Sinica* 12 (6), 710–715
- 819 Liu, J. Y., Y. I. Chen, S. A. Pulnests, Y. B Tsai, and Y. J. Chuo, (2000) Seismo-
820 ionospheric signatures prior to $M > 6.0$ Taiwan earthquakes, *Geophys. Res.*
821 *Lett.*, 27, 3113-3116, 2000.
- 822 Liu, J. Y., Y. I. Chen, C. H. Chen, and K. Hattori (2010), Temporal and spatial precursors
823 in the ionospheric global positioning system (GNSS GPS) total electron content
824 observed before the 26 December 2004 M9.3 Sumatra-Andaman Earthquake, *J.*
825 *Geophys. Res.*, 115, A09312, doi:10.1029/ 2010JA015313.
- 826 MacArthur, Steven D (1980) *Human spirit in Pauline usage*. PhD thesis, University of
827 Glasgow

828 Martinelli G, (1998), History of earthquake prediction researches, *Il NuovoCimento C*
829 22(3)

830 Mehta, A., and J. Susskind,(1999),Outgoing Longwavelength Radiation from the TOVS
831 Pathfinder Path A Data Set, *J.Geophys. Res.*, 104, NO.d10,12193-12212.

832 Milne J. (1913) Earthquakes and other movements, 2nd edition, London, 210p

833 Ohring, G. and Gruber, A.: (1982), Satellite radiation observations and climate theory,
834 *Advance in Geophysics.*, 25, 237–304, 1982.

835 Ouzounov, D., and F. Freund, (2004) Mid-infrared emission prior to strong earthquakes
836 analyzed by remote sensing data, *Adv. Space Res.*, 33(3), 268-273

837 Ouzounov D., Liu, D., Kang,C. , Cervone, G., Kafatos, M., Taylor, P. (2007), Outgoing
838 Long Wave Radiation Variability from IR Satellite Data Prior to Major
839 Earthquakes, *Tectonophysics*, 431, 211-220

840 Ouzounov D. S.Pulinets, K.Hattori, M, Kafatos, P.Taylor (2011), Atmospheric Signals
841 Associated with Major Earthquakes. A Multi-Sensor Approach, in the book
842 “Frontier of Earthquake short-term prediction study”, M Hayakawa, (Ed),
843 Japan, 510-531

844 Ouzounov D, S. Pulinets, J. Y. Liu, K. Hattori, P. Kalenda, W. Shen, V. S. Bobrovskiy,C.
845 Windsor, M. Kafatos, and P.Taylor (2011), Utilizing new methodologies to
846 study major earthquakes: Multi-parameter observation of pre-earthquake
847 signals from ground and space, *AGU Meeting Abstracts*

848 Ouzounov, D., M. Kafatos, L. Petrov, S. A. Pulinets, J. Y. Liu, Y. C. Su, and S. Chen
849 (2014), Space and Ground observations of Pre-earthquake Anomalies.
850 Prospective/Retrospective Testing for M6.0 August 24, 2014 South Napa, CA,
851 *AGU Fall Meeting Abstracts* 4942

852 Ouzounov, D., S. Pulinets, and D. Davidenko (2015a), Revealing pre- earthquake
853 signatures in atmosphere and ionosphere associated with 2015 M7.8 and M7.3
854 events in Nepal. Preliminary results, arXiv:1508.01805

855 Ouzounov D, S. Pulinets, K.Hattori, L.Lee, J.Y.Liu and M.C. Kafatos (2015b),
856 Prospective Validation of Pre-earthquake Atmospheric Signals and Their
857 Potential for Short-term Earthquake Forecasting *Geophysical Research*
858 *Abstracts* Vol. 17, EGU2015-7840-1, EGU General Assembly

859 Ouzounov D, S.Pulinets, D. Davidenko, M.Hernández-Pajares , A.García-Rigo , L.
860 Petrov, N. Hatzopoulos , M. Kafatos (2016), Pre-earthquake signatures in
861 atmosphere /ionosphere and their potential for short-term earthquake
862 forecasting. Case studies for 2015, *Geophysical Research Abstracts*, Vol. 18,
863 EGU2016-3496, EGU Assembly

864 Pergola N., Aliano C., Coviello I., Filizzola C., Genzano N., Lacava T., Lisi M., Mazzeo
865 G. and Tramutoli V. (2010) Using RST approach and EOS-MODIS radiances
866 for monitoring seismically active regions: a study on the 6 April 2009 Abruzzo
867 earthquake. *Natural Hazards and Earth System Sciences*, 10, pp.239–249

868 Pulinets S, and K. Boyarchuk (2014) *Ionospheric Precursors of Earthquakes*, Springer,

869 Pulinets S, Ouzounov, D Ciraolo L.; Singh, R.; Cervone, G.; Leyva, A.; Dunajicka, M.;
870 Karelin, A.V.; Boyarchuk, K.A.; Kotsarenko, A. (2006a) ,Thermal, atmospheric
871 and ionospheric anomalies around the time of the Colima M7.8 earthquake of
872 21 January 2003. *Ann. Geophys.* 2006, 24, 835-849.

873 Pulinets S, Ouzounov D, Karelin A, Boyarchuk K, Pokhmelnikh L,(2006b), The physical
874 nature of thermal anomalies observed before strong earthquakes, *Physics and*
875 *Chemistry of the Earth*, Volume 31, Issue 4-9, p. 143-153

876 Pulinets S and D Ouzounov, (2011), Lithosphere–Atmosphere–Ionosphere Coupling
877 (LAIC) model–An unified concept for earthquake precursors validation,
878 *Journal of Asian Earth Sciences* 41 (4), 371-382

879 Pulinets, S., and Davidenko, D ,(2014), Ionospheric precursors of earthquakes
880 and global electric circuit, *Adv. Space Res.*, 53(5), 709-723

- 881 Pulinets S., D. Ouzounov, A.Karelin, D. Davidenko (2015) Physical Bases of the
882 Generation of Short-Term Earthquake Precursors: A Complex Model of
883 Ionization-Induced Geophysical Processes in the Lithosphere–Atmosphere–
884 Ionosphere–Magnetosphere System, *Geomagnetism and Aeronomy*, 55, No.4,
885 540-558
- 886 Quing, Zu-Ji, Xu, Xiu-Deng, Dian, Chang-Gong. (1991) Thermal infrared anomaly -
887 precursor of impending earthquakes. *Chinese science bulletin*, 36: 319
- 888 Salman, A., Egan, W.G., Tronin, A.A., (1992) Infrared remote sensing of seismic
889 disturbances. In: *Polarization and Remote Sensing*. SPIE, San Diego, CA, pp.
890 208–218 (4), 319–323
- 891 Saraf, A, Choudhury, S.,(2005) NOAA-AVHRR detects thermal anomaly associated with
892 26 January,2001 Bhuj Earthquake, Gujarat, India. *Int. J. Remote Sens*, 26,
893 1065-1073
- 894 Schorlemmer D., Wiemer S., Wyss M., (2004), Earthquake statistics at Parkfield: 1.
895 Stationarity of b-values, *Journal of Geophysical Research*, 109, B12307,
896 doi:[10.1029/2004JB003234](https://doi.org/10.1029/2004JB003234)
- 897 Scholz C.H., Sykes L.R., Aggarwal Y.P. (1973), Earthquake prediction: A physical basis,
898 *Science*, 181, 803-809
- 899 Sekimoto, K., Takayama, M.(2007), Influence of needle voltage on the formation of
900 negative core ions using atmospheric pressure corona discharge in air ,
901 *International Journal of Mass Spectrometry*, 261. p. 38–44
- 902 Susskind, J., and J. Blaisdell, (2008), Improved surface parameter retrievals using
903 AIRS/AMSU data, *Proc. SPIE Int. Soc. Opt. Eng.*, 6966, 696610,
904 doi:[10.1117/12.774759](https://doi.org/10.1117/12.774759).
- 905 Tagami, T., Hasebe, N., Kamohara, H., Takemura K., (2008), Thermal anomaly around
906 the Nojima Fault as detected by fission-track analysis of Ogura 500 m borehole
907 samples. *Island Arc*, 10: 457
- 908 Tramutoli, V., Cuomo, V., Filizzola, C., Pergola, N., Pietrapertosa, C., (1999), Assessing
909 the potential of thermal infrared satellite surveys for monitoring seismically
910 active areas. The case of Kocaeli (İzmit) earthquake, August 17th, 1999,
911 *Remote Sensing of Environment*, 96 (3-4), 409-426, 2005.
- 912 Tramutoli, V., Di Bello, G., Pergola, N., and Piscitelli, S., (2001), Robust satellite
913 techniques for remote sensing of seismically active areas, *Ann. Geophys.*,
914 44(2), 295-312, 2001.
- 915 Tramutoli, V., Aliano, C., Corrado, R., Filizzola, C., Genzano, N., Lisi, M., Martinelli,
916 G., Pergola, N. , (2013), On the possible origin of Thermal Infrared Radiation
917 (TIR) anomalies in earthquake-prone areas observed using Robust Satellite
918 Techniques (RST). *Chemical Geology*, vol. 339, 157-168
- 919 Tramutoli V, Armandi B, Corrado R, Filizzola C, Genzano N, Lisi M, Paciello R, Pergola
920 N , (2014a), Long term TIR satellite monitoring over Europe, Us and Asian
921 regions: results and possible implications for an integrated system for a Time-
922 Dependent Assessment of Seismic Hazard (T-DASH). In 2014 URSI GASS
923 2014 XXXIth URSI General Assembly And Scientific Symposium 1–2. 16-23
924 Agosto 2014, Beijing. Doi: [10.1109/URSI_GASS.2014.6929870](https://doi.org/10.1109/URSI_GASS.2014.6929870).
- 925 Tramutoli V, Armandi B, Coviello I, Eleftheriou A, Filizzola C, Genzano N, Lacava T,
926 Lisi M, Paciello R, Pergola N, Satriano V, Vallianatos F, (2014b). Long Term
927 RST Analyses of TIR Satellite Radiances in Different Geotectonic Contexts:
928 Results and Implications for a Time Dependent Assessment of Seismic Hazard
929 (t-DASH). American Geophysical Union (AGU) Fall Meeting 15-19 dicembre
930 2014 San Francisco
- 931 Tramutoli V., Corrado R., Filizzola C., Genzano N., Lisi M. and Pergola N. (2015a).
932 From visual comparison to robust satellite techniques: 30 years of thermal

- 933 infrared satellite data analyses for the study of earthquake preparation phases.
934 Boll. Geof. Teor. Appl., 56 (2), 167-202,
935 Tramutoli V., Corrado R., Filizzola C., Genzano N., Lisi M., Paciello R. and Pergola N.
936 (2015b). One year of RST based satellite thermal monitoring over two Italian
937 seismic areas. Boll. Geof. Teor. Appl., 56 (2), 275-294
938 Tributsch (1978) Do aerosols anomalies precede earthquakes? Nature, 276,1978,606-607
939 Tronin, A.A.(1996), Satellite thermal survey—a new tool for the studies of seismoactive
940 regions. Int. J.Remote Sens. 1996, 17, 1439-1455.
941 Tronin, A.A.; Hayakawa, M.; Molchanov, O.A. (2002), Thermal IR satellite data
942 application for earthquake research in Japan and China. J. Geodynamics, 33,
943 519-534.
944 Tronin, A.A.; Biagi, P.F.; Molchanov, O.A.; Khatkevich, Y.M.; Gordeev, E.I., (2004),
945 Temperature variations related to earthquakes from simultaneous observation at
946 the ground stations and by satellites in Kamchatka area. Phys. Chem. Earth
947 2004, 29, 501-506
948 Tronin, A.A. ,(2006), Remote sensing and earthquakes: a review. Phys. Chem. Earth, 31,
949 138-142
950 Tronin, AA. (2011) Catalog of thermal and atmospheric phenomena associated with
951 earthquakes, Sankt Petersburg, Russia, (in Russian), 260pp
952
953